Cloud Retrieval Algorithm for the European Space Agency's Global Ozone Monitoring Experiment

T.P. Kurosu, K.V. Chance and R.J.D. Spurr

Harvard–Smithsonian Center for Astrophysics, Cambridge, Massachusetts, USA

ABSTRACT

The Global Ozone Monitoring Experiment (GOME) on board the ERS-2 satellite is an across-track nadir-viewing spectrometer which measures solar light reflected from the Earth's atmosphere and surface in the UV visible. The cloud retrieval algorithm presented here combines spectral threshold tests on GOME's broad-band radiances (∼150 nm spectral resolution) with the fitting of reflectances to GOME's moderately high resolution spectra (0.4 nm) in and around the O_2 *A* band to retrieve cloud-cover fraction, cloud-top height and cloud optical thickness. The algorithm utilizes the latest O_2 spectroscopic data and features dynamical updating procedures to provide global threshold sets of GOME reflectances. Auxiliary information is obtained from GOME measurements of the Ring effect and the degree of polarization of the Earth's radiation field.

Keywords: Cloud detection, cloud retrieval, satellite remote sensing, GOME

1. INTRODUCTION

Satellite instruments measuring atmospheric change in the UV, visible and infrared spectral range are strongly influenced by the presence of clouds in Earth's atmosphere. Failure to account for this presence can result in large errors in the interpretation of measurement data. Reliable cloud detection techniques are therefore crucial for monitoring the Earth's atmosphere from space in nadir viewing mode.

The European Space Agency's (ESA) Global Ozone Monitoring Experiment is an ESA core instrument on board the second European Remote Sensing (ERS-2) satellite.[1] GOME measures reflected and back scattered radiation from 238 to 794 nm at moderately high resolution (0.2 nm in the ultraviolet and 0.4 nm in the visible and near infrared). The variable swath width of the across-track scan provides ground footprints from 40×40 km^2 to 40×320 km^2. The largest swath width, which is obtained in the standard mode of operation, provides full global coverage in three days. A summary of the characteristics of GOME's detectors is given in Table 1.

In addition to the high resolution spectrometer, GOME carries three polarization measurement devices (PMDs, see Table 1 for specifications). During the read-out of the standard detector array, each of these broad-band detectors (spectral resolution 100–200 nm) takes 16 measurements of the Earth's radiance with polarization parallel to the instrument slit. In the standard mode of operation, the PMD measurements have a ground footprint of 40×20 km^2.

The scientific objectives of GOME are the accurate global measurement of atmospheric constituents (trace gases, aerosols and clouds) and the surface spectral reflectances. Demonstrated gas measurements from GOME now include O_3, NO_2, BrO, OClO, ClO, SO_2, NO, H_2CO, and H_2O. Measurements of O_3 include total column amounts, vertical profiles (both stratosphere and troposphere), and tropospheric ozone.[2–7]

The Cloud Retrieval Algorithm for the GOME instrument (CRAG) will provide a fast and reliable tool for cloud detection. Once completed, CRAG will become part of the operational GOME data processing chain, but will also be accessible as a

GOME Spectral Detectors

Band	Spectral range [nm]	Integration time [s]	Spectral res. [nm]	Spatial res. [km^2]
1A	238–307	12	0.22	100×960
1B	307–314	1.5		40×320
2A	311–312		0.24	
2B	312–404			
3	394–611		0.40	
4	578–794			

GOME Polarization Detectors

Band	Spectral range [nm]	Integration time [ms]	Spectral res. [nm]	Spatial res. [km^2]
1	295–397	98	102	40×20
2	397–580		183	
3	580–745		165	

Table 1. Characteristics of the GOME detectors.

Other author information: Send correspondence to tkurosu@cfa.harvard.edu

stand-alone tool for users of GOME data.* The aim of CRAG is the retrieval of the following cloud parameters from GOME data: cloud fraction, cloud-top height and, possibly, cloud optical thickness. Presently, the cloud fractional coverage for a GOME standard pixel can be retrieved with high confidence using a threshold method applied to the GOME PMDs. The retrieval of cloud-top height and cloud optical thickness, based on a fitting procedure using GOME radiances in and around the *A* band of oxygen, is still under development. These and other aspects of the CRAG algorithm will be described in Section 2, while in Section 3 we demonstrate a case study of the application of CRAG to a hurricane scenario.

2. DESIGN OF THE CRAG ALGORITHM

2.1. Existing Work Prior to this Study

The method used in the first cloud recognition algorithm for GOME was developed by *Kuze and Chance*.[8] The Initial Cloud Fitting Algorithm (ICFA), which has been implemented as one of the component algorithms in the operational GOME data processing chain,[9] employs multi-linear regression of GOME radiances against simulated values in and around the O_2 *A* band for the detection of cloud fraction in a GOME pixel. Cloud-top height information is taken from an ISCCP climatological data base.[10] ICFA cloud fraction values are included in the GOME level 2 data product.

A number of cloud detection techniques using GOME data were investigated by *Deschamps* et al.[11] They proposed a cloud detection algorithm based on a combination of O_2 *A* band fitting and spectral threshold tests based on the spectrally broader, but spatially higher resolved PMD signals. In a follow-up study,[12] a first version of a GOME-PMD cloud detection algorithm was realized by one of the present authors.[13] The PMD Cloud Recognition Algorithm (PCRA) for CRAG presented here is based in part on this original PMD cloud detection algorithm.

2.2. Overview

CRAG combines information from GOME channels for the retrieval of cloud fractional cover, cloud-top height and cloud optical thickness from GOME data. The use of auxiliary information from cloud climatologies such as ISCCP[10] can help to retrieve cloud type. Figure 1 gives an overview of the main elements of the algorithm and their interrelationship.

Currently the two main elements are the PCRA, retrieving primarily cloud-cover fraction, and a χ^2 grid-search procedure, which retrieves cloud-top height and cloud optical thickness by comparing high spectral resolution GOME radiances in and around the oxygen *A* band with simulated radiances created with a radiative transfer model. The PCRA and the χ^2 procedure will be described in detail in the following sections. Auxiliary information on clouds may be obtained from "Ring" scattering and the degree of polarization in a GOME pixel. This task is under development and has not yet been interfaced with CRAG.

CRAG is written entirely in Fortran 90 and has been developed and tested in a Sun Solaris® environment. Full use has been made of the Fortran 90 capability to define precision for integer and real variables; this makes CRAG readily portable to other platforms.

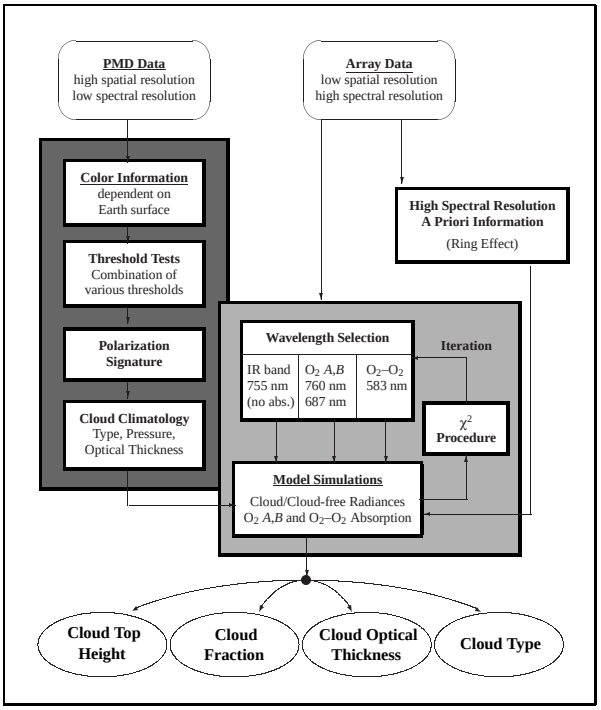

Figure 1. Overview of the CRAG algorithm

2.3. PCRA for Cloud Fraction

2.3.1. Spectral threshold tests

The basic idea behind a spectral threshold is that, while the Earth's surface reflects light with a strong spectral, surface-dependent signature, clouds are almost perfect scatterers in the visible region (the wavelength dependence of Mie scattering is proportional to $\sim \lambda^{-1}$; also, in the spectral region of GOME, the single scattering albedo of water droplets is very close to 1.0). A pixel that is contaminated by clouds will have a higher detector signals than one that is cloud-free. Since the three GOME PMDs cover the visible spectral regions of blue (PMD_1), green (PMD_2) and red (PMD_3) respectively (see Table 1), flexible threshold techniques can be adopted, depending on the underlying Earth's surface.

*CRAG is freely available for public use. Interested users can obtain the algorithm by sending an EMail request to the authors.

Figure 2 shows the general layout of the PMD threshold detection process. The 16×3 PMD measurements P_i^{bgr}, $i = 1, \ldots, 16$, for a given GOME pixel, with the super-scripts *bgr* indicating the blue, green and red PMD, are compared with predefined threshold values $P_{\mathrm{min,max}}^{bgr}$. The retrieval of cloud-free and completely cloudy PMD sub-pixels is then performed as follows:

$$\text{PMD Subpixel } i = \begin{cases} \text{clear}, & P_i^{bgr} \leq P_{\mathrm{min}}^{bgr} + \delta_{\mathrm{min}}^{bgr}, \\ \text{cloudy}, & P_i^{bgr} \geq P_{\mathrm{max}}^{bgr} - \delta_{\mathrm{max}}^{bgr}, \end{cases} \tag{1}$$

where $\delta_{\mathrm{min,max}}^{bgr}$ are threshold margins, which are specified as fractions of the $P_{\mathrm{min,max}}^{bgr}$ and which can be varied to tune the performance of the algorithm: larger (smaller) values of $\delta_{\mathrm{min,max}}^{bgr}$ will lead to more (less) pixels being classified as either cloud free or completely cloudy.

Test (1) will fail for $P_{\mathrm{min}}^{bgr} + \delta_{\mathrm{min}}^{bgr} < P_i^{bgr} < P_{\mathrm{max}}^{bgr} - \delta_{\mathrm{max}}^{bgr}$. This typically happens for pixels with a partially cloud cover. In such cases the cloud cover (or "cloudiness") fraction f of the pixel is computed according to

$$f = \frac{|P_i^{bgr} - P_{\mathrm{min}}^{bgr}|}{P_{\mathrm{max}}^{bgr} - P_{\mathrm{min}}^{bgr}}. \tag{2}$$

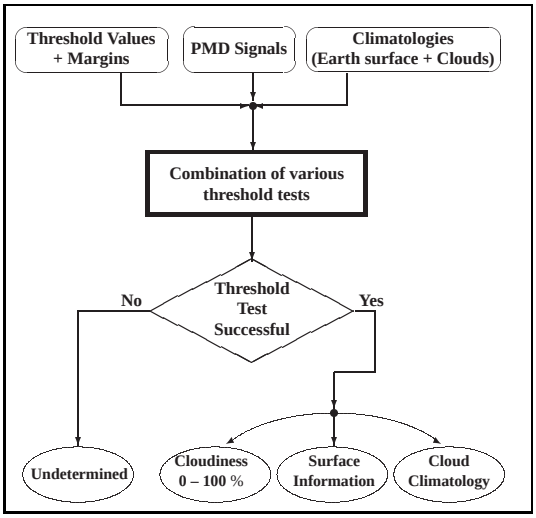

Figure 2. Overview of the PCRA.

The threshold tests are designed to use PMD_2 measurements over land surfaces and PMD_3 over the ocean. PMD_1 data is regarded as a fall-back, since it is the channel most corrupted by Rayleigh scattering. In addition to threshold tests on the absolute PMD signals, the color ratio $R = \mathrm{PMD}_3/\mathrm{PMD}_2$ is included in the tests. For cloudy scenarios, one expects $R \approx 1$, while for cloud-free conditions one finds $R \gtrless 1$ depending on the type of the Earth's surface. In a cloud-free land scenario, for example, more green light than red is reflected, which leads to $R > 1$. Over oceanic areas, on the other hand, the situation is reversed and cloud-free pixels are characterized by $R < 1$.

2.3.2. PCRA threshold sets

The crucial elements in the relations (1) and (2) are the threshold values $P_{\mathrm{min,max}}^{bgr}$. It has been demonstrated by *Fouquart* et al.[11] that the use of static thresholds, i.e., $P_{\mathrm{min,max}}^{bgr}$, that are chosen at the outset, can lead to large errors in the retrieved cloud fraction. A reliable cloud recognition requires the repeated update of thresholds using real measurement signals from clear and fully cloudy scenes. This *dynamic* update procedure starts with a fixed set of thresholds $P_{\mathrm{min,max}}^{(0)}$; each time a pixel with signal P_i is detected as clear (cloudy), a check for $P_i^{bgr} < P_{\mathrm{min}}^{(0)}$ ($P_i^{bgr} > P_{\mathrm{max}}^{(0)}$) is performed and, if true, $P_{\mathrm{min}}^{(0)}$ (respectively $P_{\mathrm{max}}^{(0)}$) is replaced by P_i^{bgr}. After a sufficiently large number n of updates, the resulting $P_{\mathrm{min,max}}^{bgr} = P_{\mathrm{min,max}}^{(n)}$ will represent signals originating from clear and cloudy pixels.

A large data base of minimum and maximum PMD reflectances has been compiled and interfaced to CRAG. For each month of the complete period of GOME data distribution to date (07/95–05/98), global sets of PMD threshold have been computed, each containing minima and maxima of all three PMDs as well as the color ratio R, for a spatial resolution of $0.5^\circ \times 0.5^\circ$ on the Earth's surface. This data set is extended with each newly processed month of complete GOME data. The monthly thresholds can in turn be combined into a single data set for the whole lifetime of GOME, resulting in a threshold set with minimum cloud contamination and ice and snow cover.

2.4. χ^2 Procedure for Cloud-Top Height

The detection of cloud-top height is based on the variability of reflectances in and around the oxygen absorption bands in the visible and near infrared regions.[14,15] This signature is caused by differences in the amount of oxygen seen by the light on its way to the detector. A cloud, especially when optically thick, will effectively cut off parts of the atmosphere below the cloud-top and will therefore reduce the amount of oxygen that can absorb light. As a result, the normalized reflectance, i.e., the radiances inside the absorption band normalized to an out-of-band radiance, will increase. Figure 3 illustrates this for a cloud-free scenario and a number of cloudy scenes which contain the same cloud (optical thickness, type) at various altitudes between 2.5 and 12.0 km.

It should be noted that the neglect of light scattering inside the cloud can lead to a significant error in the retrieved cloud-top height. Since in-cloud multiple scattering enhances the atmospheric light path,[16] oxygen absorption is also enhanced and, as a consequence, the retrieved cloud-top will be too low.

Assuming the cloud fraction in a GOME pixel is known, cloud optical thickness can be fitted as an additional parameter. Due to the possible correlation of cloud-top height and cloud optical thickness, care must be taken to distinguish between the effects of these parameters on the measured radiances. In the final version of CRAG cloud-top height and cloud optical thickness will be retrieved using non-linear inverse methods. This is still under development, and at present we use a χ^2 grid search as a preliminary method. Here, GOME radiances are compared against pre-computed templates of top-of-atmosphere (TOA) radiances. The result of the grid search retrieval is the combination (h, τ) of cloud-top height and cloud optical thickness, which yields the lowest χ^2. A set of simulated TOA radiances for various cloudy and non-cloudy scenarios has been computed using a full multiple scattering radiative transfer model, which includes a line-by-line treatment of *A* band absorption, and an accurate parameterization of clouds. GOMETRAN, a radiative transfer model specifically developed for the interpretation of GOME data,[17] contains quasi-exact and approximate methods to simulate cloud radiative transfer[16] and has been modified for the CRAG study to include a new spectroscopic data set of the O_2 *A* band, based on the latest oxygen laboratory measurements.[18] The latter include the effects of pressure-induced shifts in line position. GOMETRAN is thus eminently suited to the present task. However, computation times are long when clouds are included. Even with a fast approximation for cloud scattering, a complete line-by-line computation covering the O_2 *A* band exceeds two hours on a Sun Ultra 2 workstation.

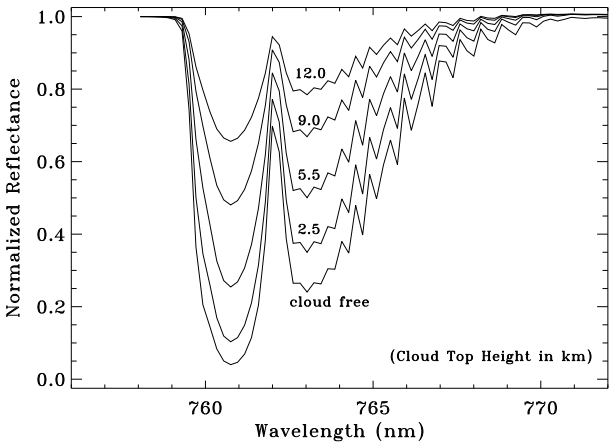

Figure 3. Comparison of normalized reflectances in the O_2 *A* band for a cloud-free scenario with scenes containing the same cloud at various altitudes. Viewing geometry and cloud parameters other than cloud-top altitude are identical in all scenes. Reflectances are shown with GOME spectral resolution.

For proper comparison with measurements, high resolution simulated reflectances must be convoluted to GOME wavelengths. At present, the templates are calculated for two surface albedos (0%, 30%), two solar zenith angles (20°, 50°), four line-of-sight angles between 0° and 45° (covering GOME's maximum scan angle range of ±30°), five cloud-top altitudes between 0.5 and 12.0 km, and five values of cloud optical thickness between 15 and 500. Akima interpolation[19] is used to interpolate the template data to intermediate grid points. Some examples of the final shape of the synthetic convoluted GOMETRAN O_2 spectra have been shown in Figure 3.

2.5. Auxiliary Information from GOME Data

2.5.1. Polarization

Light that has been scattered in a cloud possesses varying polarization characteristics, depending on the main particulate constituents of the cloud. While water droplets (tropospheric water clouds) depolarize, ice particles (cirrus) lead to a strong polarization signature in the scattered light. In combination with cloud parameters retrieved from the PCRA and the χ^2 grid search this information could be used, for example, in the detection of cirrus clouds or low clouds over highly reflecting surfaces.

The degree of polarization in a GOME pixel is contained in the GOME data product. This quantity is computed from a comparison of PMD signals, which measure the part of the radiation field with a polarization component parallel to the instrument's slit, with the unpolarized signals of the detectors with high spectral resolution. A major source of error in the use of GOME polarization measurements for cloud detection is the accuracy of this polarization correction procedure. As will be seen in Section 3, polarization in a GOME pixel does correlate to some extent with retrieved cloud presence.

2.5.2. Ring effect

The Ring effect[20] was first observed as a broadening and reduction in depth of solar Fraunhofer lines when viewed from the ground. For measurements at GOME and similar satellite geometries it has been determined that the dominant contribution to the Ring effect is from the inelastic component of Rayleigh scattering, which is mostly rotational Raman scattering.[21–23] The utilization of the Ring effect for cloud detection was first suggested by *Joiner and Bhartia*.[24] The distortion of the

solar Fraunhofer spectrum by convolution of the inelastically-scattered portion of the Rayleigh scattering with the N_2 and O_2 rotational Raman spectra is proportional to the number of Rayleigh scattering incidences the light has experienced. This signature can be utilized to retrieve cloud-top height in a similar manner to that used in the absorption bands of oxygen: the effect of rotational Raman scattering will generally be reduced by the presence of clouds, and higher clouds lead to more reduction than low clouds. A similar argument holds for the determination of cloud fraction.

For the present study, GOME wavelengths around the Ca H and K lines, centered at wavelengths 397.0 and 393.5 nm respectively, have been used to determine cloud fraction. This is accomplished using a simple algorithm: first, template spectra are selected from GOME measurements taken with the correct viewing geometry and which can be characterized as either fully cloudy or clear; the shape of the selected spectral region for other GOME spectra is then fitted as a linear combination of the cloudy and clear template spectra, As will be shown in Section 3, the results obtained from this preliminary Ring fitting are strongly correlated to those from the PCRA.

3. CRAG APPLICATION: A HURRICANE SCENARIO

This section presents a case study of the application of CRAG. The choice of a hurricane scenario provides the opportunity to study a number of relevant atmospheric variables (amounts of cloud cover and optical thickness, various surface conditions) over a relatively small spatial scale. There is a wealth of synoptic and satellite information available from national hurricane data centers. The particular hurricane scenario presented here (Hurricane Fran on September 4, 1996) has the additional advantage of near-simultaneous over-passes of GOES-8 (16:02 UTC) and GOME (16:04 UTC).

During the period of September 4–8 1996, Hurricane Fran hit the eastern United States. The event received intense media coverage and was monitored in detail by NOAA's GOES-8 satellite.[†] Figure 4 shows a GOES-8 image of Fran at 16:02 UTC on September 4[‡], just before its land-fall in Southeast North Carolina on September 5. At 15:00 UTC, Fran was located at 27.4°N,75.0°W with a recorded ground pressure of 956 mb. [§] By estimating surface and cloud-top temperatures from color-enhanced infrared images of the GOES-8 satellite[¶] to be ca. $+15$°C and -60°C (central part, north of the eye) respectively, Fran's cloud-top altitude is found to be $\sim$7.5 km. For the outer parts of the hurricane, an inferred -25° cloud-top temperature corresponds to $\sim$3.7 km cloud-top height.

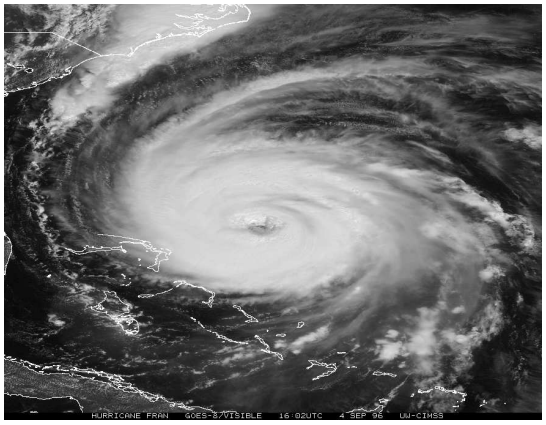

Figure 4. Hurricane FRAN at 16:02 UTC on 09/04/96, from NOAA's GOES-8 satellite.

A view of Fran as seen by the GOME PMDs is shown in Figure 5 (left image). Signals from all three PMD detectors have been combined to produce a grey-scale composite of the scene. Despite the coarser spatial resolution of GOME, all main features of Fran and its surrounding cloud field can be identified. In the following subsections the results from CRAG for this scenario are presented in the order they are produced by the algorithm. Results from the retrieval of cloud fraction from the PCRA are used in the retrieval of cloud-top height and cloud optical thickness from the χ^2 grid search. Additional results from Ring fitting and the degree of polarization in the GOME signals are presented for completeness.

3.1. PCRA Results for the Fran Event

The first step of CRAG processing consists of the determination of cloud fractional cover using the GOME PMDs. Figure 5 shows the result from the PCRA at PMD resolution (20×40 km^2, middle plot) and GOME standard pixel resolution (320×40 km^2, right). The latter is computed as the average over the 16 PMD sub-pixels. The choice of grey-scale in Figure 5 is such that higher cloud fraction values are represented by brighter values, making pixels with optically thick clouds appear white.

Qualitative comparison of the PCRA results with the GOES-8 image in Figure 4 shows that the PCRA correctly recognizes the main characteristics of the scenario. Due to the viewing geometry and the limit in PMD spatial resolution, the eye of the hurricane, which would appear as a small cloud-free area if seen directly from above, shows as a PMD sub-pixel of lower cloud cover than the surrounding hurricane. Also, the transition from oceanic to continental surfaces is reproduced correctly by the

[†] See *http://www.ncdc.noaa.gov/fran.html* and *http://www.nhc.noaa.gov/1996fran.html* for detailed information about the Fran event.
[‡] Source: http://www.wmo.ch/web/wiscssec/figures/96season/FRAN6.GIF
[§] *http://www.nhc.noaa.gov/1996fran.html*
[¶] *http://www.ncdc.noaa.gov/pub/data/images/hurricane-fran-ir-sep04.gif* and *http://www.ncdc.noaa.gov/psguide/satellite/tstorm1.gif*

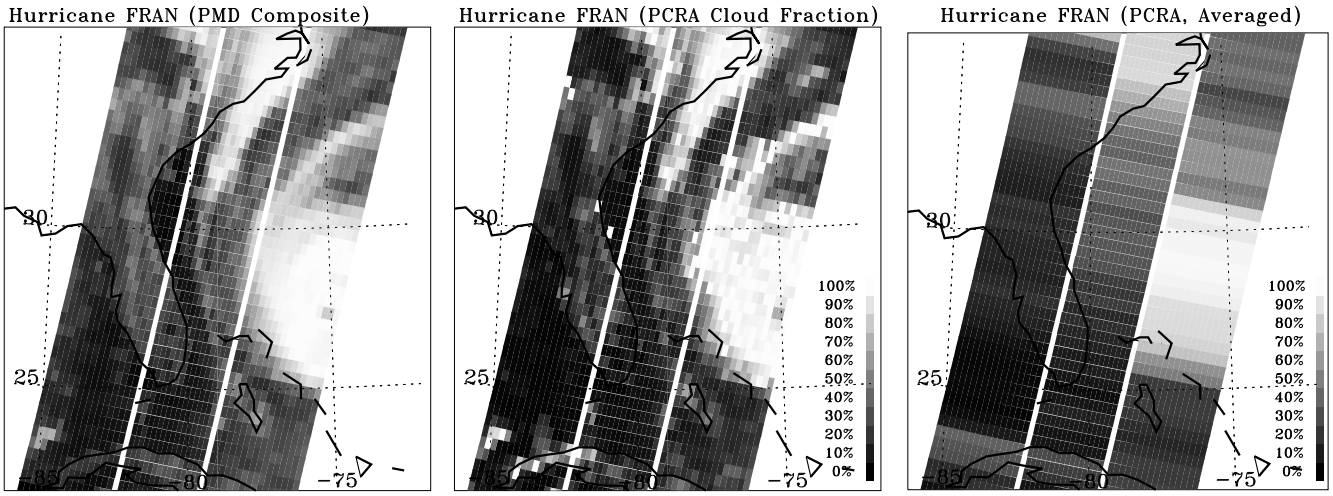

Figure 5. Hurricane FRAN on 09/04/96, as seen by GOME at 16:04 UTC. Left: PMD composite; middle: PCRA cloud-cover results; right: average of the 16 PMD sub-pixel values.

PCRA. The scattered PMD pixels of low cloud cover over Florida are due to small scale cloud features that cannot be resolved by the PMDs.

It should be noted that the retrieved fractional coverage has to be regarded as an "effective" cloud cover, since threshold tests at sub-pixel scale are unable to discriminate between a PMD pixel covered completely with an optically thin cloud or only partly with a thicker cloud (same brightness values). This consideration also applies to GOME's high spectral resolution measurements used for the determination of cloud-top height and cloud optical thickness.

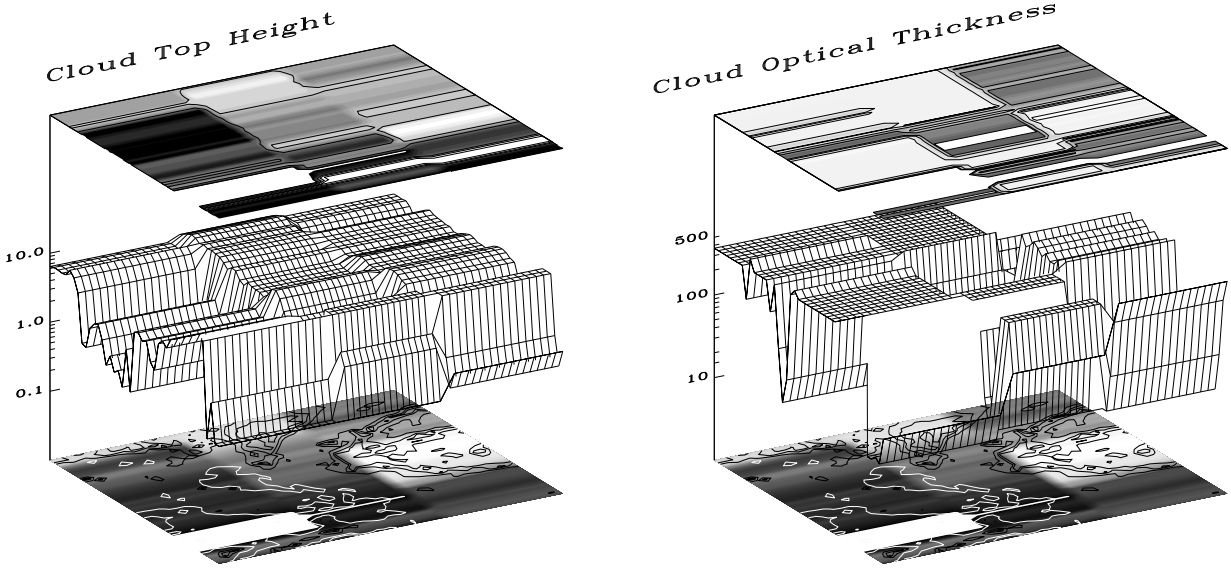

Figure 6. Surface plots for cloud-top height h and cloud optical thickness τ for Hurricane Fran, as retrieved from χ^2 grid search. In both plots, the retrieved parameter is visualized as a surface mesh, which is overlaid by its own contour plot and underlaid by a contour plot of the averaged cloud fraction f (averaged PCRA results) along with PCRA contours for visual orientation. Blank areas represent pixels with $f < 5\%$. Contour lines in the overlay image mark values of h = 1, 5, 8 and 12 km, and τ = 16, 50, 150, 350 and 450.

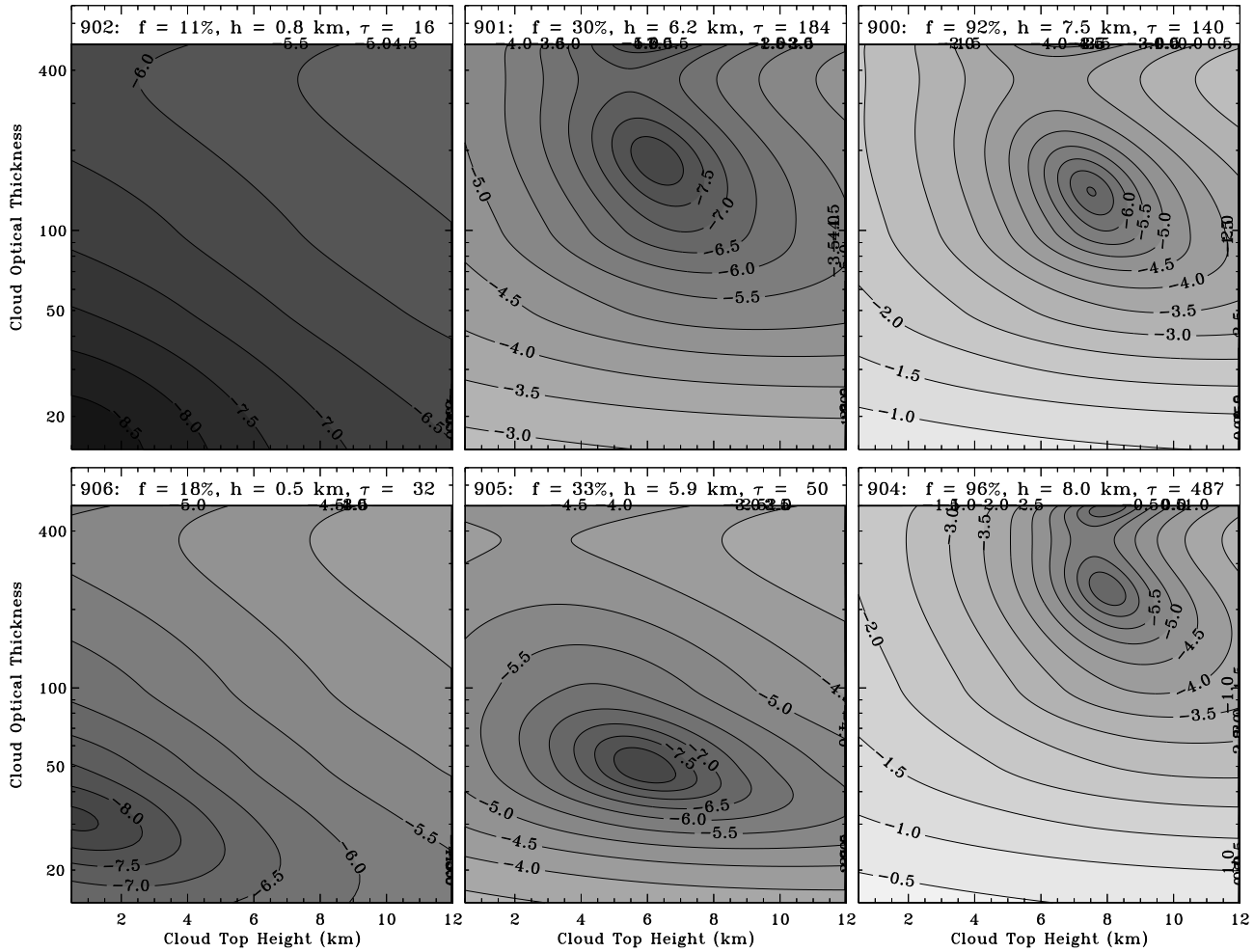

Figure 7. Contour plots of χ^2 for cloud-top height and cloud optical thickness for GOME pixels 900–906. The contour lines show $\ln\chi^2$; each contour line defines the error on the retrieved parameters. The top bar of each plot shows GOME pixel number, PCRA cloud fraction f, and the retrieved cloud-top height h and optical thickness τ. The inset shows an excerpt from Figure 5 including GOME pixel numbers.

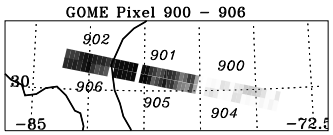

3.2. CRAG Results for Cloud-Top Height and Optical Thickness

Cloud-top height h and cloud optical thickness τ are retrieved from GOME data by the χ^2 grid search described in Section 2.4, with cloud-cover fraction of the pixel taken as the averaged result from the PCRA. Figure 6 shows the results for h and τ for the complete Fran scenario. In each plot, the retrieved cloud parameter is visualized by a surface mesh, which is overlaid by a contour plot of itself. The grey-scale coding is such that lighter shades represent larger values of either h or τ within the limits given by the currently available data base (i.e., $0.5 \leqslant h \leqslant 12$ km, $15 \leqslant \tau \leqslant 500$, see Section 2.4). Additional contour lines in the overlay image represent certain values of h and τ (see caption of Figure 6). For orientation purposes, a contour image of the pixel-averaged value of the cloud fractional cover f is shown at the bottom of each plot, overlaid by contour lines from the original PMD signals that give a better outline of the hurricane and the adjacent land mass. In both plots, missing data represent GOME standard pixels with $f < 5\%$, for which no χ^2 grid search has been performed.

Details of the output from the χ^2 grid search for six adjacent GOME pixels are shown in Figure 7. The pixels are located slightly north of Fran's eye but still within the central part of the hurricane (the inset shows their location with respect to the complete scene in Figure 5). The pixels have areas of high, medium and low cloud cover and there is also a transition from ocean to land surface; this is then a reasonable cross-section of the hurricane.

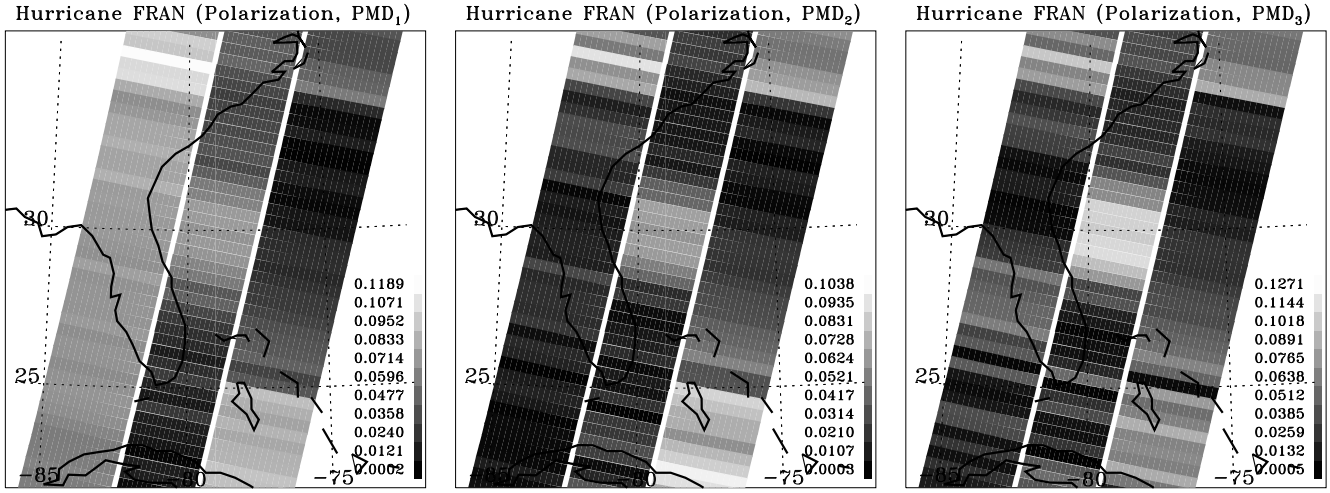

Figure 8. Degree of polarization in a standard GOME pixel for the Fran scenario. From left to right, GOME polarization is shown for the three wavelengths 355, 490 and 702 nm, lying within the spectral ranges of PMDs 1–3 respectively.

Each plot in Figure 7 contains filled contour lines of the χ^2 grid search over h and τ for a single GOME pixel, with contour labels showing $\ln\chi^2$. The choice of grey scale is such that darker areas represent lower values of $\ln\chi^2$. At the top of each plot, GOME pixel number, f and the combination of h and τ that produced the smallest χ^2 are given. It is apparent that well-defined minima exist for all six scenes. In pixels with high values of retrieved cloud optical thickness (pixels 900, 901 and 904), a second local minimum appears, indicating some ambiguities in the (h,τ) results. Only the retrieved cloud-top height can be compared quantitatively with results from other satellites. As mentioned above, values for h derived from GOES-8 images are $\sim$7.4 km for the center and $\sim$3.7 km for outer regions of the hurricane field. The former value compares well with the retrieved altitudes of 7.5 km (pixel 900) and 8.0 km (pixel 904), while the latter is significantly lower than the 6.2 and 5.9 km found in pixels 901 and 905. However, it has to be kept in mind that, due to GOME's large ground pixel size, CRAG can only retrieve "effective" values for h and τ for partially cloudy pixels (note that pixels 901 and 905 have a fractional cloud coverage of $\sim$30%). Finally, for the relatively clear scenes 902 and 904, reasonably low values for h and τ are retrieved.

At this point it is not possible to perform a quantitative error analysis of the CRAG results. This is due in part to the general lack of accurate data sources of cloud-top height and especially cloud optical thickness, and in part to the current developmental status of CRAG. The main sources of errors, however, can be specified: (1) GOME's large ground pixel size, which permits the retrieval of "effective" values only for f, h and τ (see above); (2) the limited set of simulated reflectances; more radiative transfer template simulations are required to investigate the effects of thin clouds (including cirrus) and aerosols, and the reflection properties of various Earth surface types have to be considered in greater detail; (3) ambiguity in the retrieval; for example, the retrieved values of $h = 8.0$ km, $\tau = 487$ in pixel 904 has an associated $\ln\chi^2$ of -6.928; $\tau = 239$ for the same h, on the other hand, has a $\ln\chi^2$ value of -6.926.

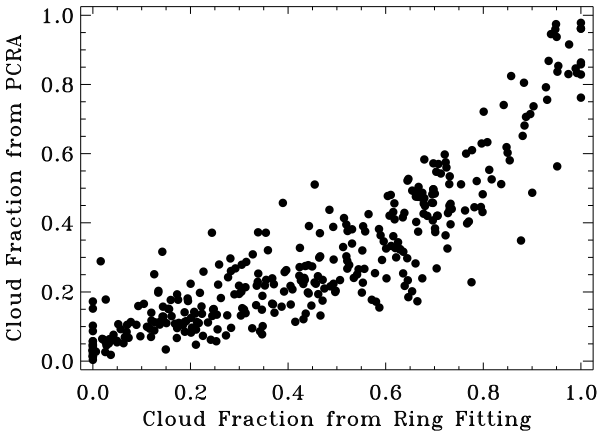

Figure 9. Cloud fraction from Ring fitting vs. PCRA.

3.3. Auxiliary Cloud Information from GOME Data

Auxiliary information from GOME are currently not included in CRAG. However, the use of the Ring effect and the degree of polarization in a standard GOME pixel are possible candidates for future versions of the algorithm. Figure 8 shows the degree of polarization in a GOME pixel (choice of grey scale as before), computed directly from the GOME level 1 data product at three wavelengths that fall into the spectral ranges of the PMD detectors. Even though a general correspondence between high cloud cover and low degree of polarization can be observed for all three wavelengths, no strong evidence for a correlation with

the cloud field exists. A more extensive study of various atmospheric scenarios, together with a proper assessment of GOME's polarization correction algorithm, needs to be performed.

Retrieval of cloud fractional cover from Ring signatures, on the other hand, appears to be more promising. The scatter plot of f_{Ring} versus f_{PCRA}, shown in Figure 9, indicates a strong correlation between the two parameters. We are currently looking at the use of f_{Ring} in those scenarios where f_{PCRA} is unreliable (snow/ice surfaces). Also, when the nature of this correlation between Ring and PCRA results has been established, the Ring effect fitting might be used in combination with oxygen absorption to improve the retrieval of cloud-top height and cloud optical thickness.

ACKNOWLEDGMENTS

This work has been funded by the European Space Agency and DLR–DFD. The authors would like to thank their colleagues at ESTEC and DLR–DFD for helpful discussions.

REFERENCES

1. G. Duchossois and R. Zobl, "ERS-2: A Continuation of the ERS-1 Success." Reprint ESA Bulletin No. 83, 1995.
2. K. Bramstedt, K.-U. Eichmann, M. Weber, V. Rozanov, R. Hoogen, R. de Beek, M. Buchwitz, T. Kurosu, and J. Burrows, "Ozone Profiles from GOME Satellite Data – Part II: First Results from the Arctic Winter Campaign," in *Proceedings of the Fourth European Symposium on Stratospheric Ozone Research*, (Schliersee), 1997.
3. J. Burrows, M. Weber, K.-U. Eichmann, K. Bramstedt, A. Richter, R. Hoogen, A. Ladstätter-Weißenmayer, and M. Buchwitz, "GOME/ERS-2 Total O_3 and NO_2 Measurements during Arctic Spring 1996 and 1997," in *Proceedings Fourth European Symposium on Stratospheric Ozone Research*, (Schliersee), 1997.
4. K. Chance, J. Burrows, D. Perner, and W. Schneider, "Satellite measurements of atmospheric ozone profiles, including tropospheric ozone, from UV/visible measurements in the nadir geometry: A potential method to retrieve tropospheric ozone," *Journal of Quantitative Spectroscopy and Radiative Transfer* **57**, pp. 467–476, 1997.
5. M. Eisinger, J. Burrows, A. Richter, and A. Ladstätter-Weißenmayer, "SO_2, OClO, BrO, and other minor trace gases from the Global Ozone Monitoring Experiment (GOME)," in *Proceedings of the Third ERS Symposium*, vol. SP-414, (Florence), March 1997.
6. K. Chance, "Analysis of BrO Measurements from the Global Ozone Monitoring Experiment," *Geophysical Research Letters* **25**(17), pp. 3335–3338, 1998.
7. R. Munro, R. Siddans, W. Reburn, and B. Kerridge, "Direct measurement of tropospheric ozone distributions from space," *Nature* **392**, pp. 168–171, 1998.
8. A. Kuze and K. Chance, "Analysis of Cloud Top Height and Cloud Coverage from Satellites Using the O_2 *A* and *B* Bands," *Journal of Geophysical Research* **99**, pp. 14,481–14,491, 1994.
9. D. Loyola, B. Aberle, W. Balzer, K. Kretschel, E. Mikusch, H. Muehle, T. Ruppert, C. Schmid, S. Slijkhuis, R. Spurr, W. Thomas, T. Wieland, and M. Wolfmueller, "Ground segment for the ERS-2 GOME sensor at the German D_PAF," in *Proceedings of the Third ERS Symposium*, vol. SP-414, pp. 591–596, (Florence), March 1997.
10. W. Rossow, A. Walker, D. Beuschel, and M. Roiter, "International Satellite Cloud Climatology Project (ISCCP) Documentation of New Cloud Datasets," Tech. Rep. WMO/TD-No. 737, World Meteorological Organization, 1996.
11. P.-Y. Deschamps, Y. Fouquart, D. Tanre, M. Herman, J. Lenoble, J. Buriez, P. Dubuisson, F. Parol, C. Vanbauce, H. Grassl, and M. Kollewe, "Study on the Effects of Scattering on the Monitoring of Atmospheric Consitutents," Tech. Rep. 9740/91/NL/BI, European Space Agency, ESA/ESTEC, The Netherlands, 1994.
12. R. Guzzi, J. Burrows, M. Cervino, and T. Kurosu, "GOME Cloud and Aerosol Data Products Algorithms Development (CADAPA)," Tech. Rep. 11572/95/NL/CN, European Space Agency, ESA/ESTEC, Noordwijk, The Netherlands, 1998.
13. T. Kurosu and J. Burrows, "PMD Cloud Detection Algorithm for the GOME Instrument – Algorithm Description and Users-Manual," Tech. Rep. 11572/95/NL/CN, European Space Agency, ESA/ESTEC, Noordwijk, The Netherlands, 1998. Annex to the ESA CADAPA Report.
14. F. Saiedy, H. Jacobowitz, and D. Wark, "On Cloud-Top Determination from Gemini-5," *Journal of the Atmospheric Sciences* **24**, pp. 63–69, 1967.
15. J. Fischer and H. Grassl, "Detection of Cloud-Top Height from Backscattered Radiances Within the Oxygen *A* Band. Part 1: Theoretical Study," *Journal of Applied Meteorology* **30**(9), pp. 1245–1259, 1991.
16. T. Kurosu, V. Rozanov, and J. Burrows, "Parameterization Schemes for Terrestrial Water Clouds in the Radiative Transfer Model GOMETRAN," *Journal of Geophysical Research* **102**(D18), pp. 21,809–21,823, 1997.

17. V. Rozanov, D. Diebel, R. Spurr, and J. Burrows, "GOMETRAN: A radiative transfer model for the satellite project GOME, the plane-parallel version," *Journal of Geophysical Research* **102**, pp. 16,683–16,695, July 1997.
18. D. Newnham and J. Ballard, "Visible absorption cross-sections and integrated absorption intensities of molecular oxygen (O_2 and O_4)." *Journal of Geophysical Research*, in press.
19. D. Hilberg, "Akima-Interpolation, Noch besser als das Spline-Verfahren," *ct* **Heft 6**, 1989. in German.
20. J. Grainger and J. Ring, "Anomalous Fraunhofer line profiles," *Nature* **193**(762), 1962.
21. G. Kattawar, A. Young, and T. Humphreys, "Inelastic scattering in planetary atmospheres. I. The Ring effect, without aerosols," *Astrophysical Journal* **243**, pp. 1049–1057, 1981.
22. J. Joiner, P. Bhartia, R. Cebula, E. Hilsenrath, R. McPeters, and H. Park, "Rotational Raman scattering (Ring effect) in satellite backscatter ultraviolet measurements," *Applied Optics* **34**, pp. 4513–4525, 1995.
23. K. Chance and R. Spurr, "Ring Effect Studies: Rayleigh scattering, including molecular parameters for rotational Raman scattering, and the Fraunhofer spectrum," *Applied Optics* **36**, p. 5224, 1997.
24. J. Joiner and P. Bhartia, "The determination of cloud pressures from rotational Raman scattering in satellite backscatter ultraviolet measurements," *Journal of Geophysical Research* **100**, pp. 23,019–23,026, November 1995.